# Synthesis and Characterization of Ru(II)−DMSO−Cl−Chalcone Complexes: DNA Binding, Nuclease, and Topoisomerase II Inhibitory Activity

Ruchi Gaur and Lallan Mishra*

Department of Chemistry, Faculty of Science, Banaras Hindu University, Varanasi-221005, India

S *Supporting Information*

ABSTRACT: The complexes of type *cis*-[Ru(S-DMSO)$_3$(R—CO—CH=CH—R′)Cl] (R = 2-hydroxyphenyl for all, R′ = phenyl **1**, naphthyl **2**, anthracenyl **3**, thiophene **4**, 3-methyl thiophene **5**) are synthesized and characterized using spectroscopic (IR, ^{1}H and ^{13}C NMR, and UV−vis) and single crystal X-ray diffraction techniques. Their crystal structures show the formation of both intermolecular and intramolecular H-bonding. The molecular assembly of complex **5** using secondary interactions provides a butterfly structure. The binding of complexes with calf thymus DNA is monitored using UV−vis spectral titrations. The binding interaction of complexes **1**, **2**, and **3** with DNA increases with increasing conjugation of aromatic rings. However, complexes **4** and **5** interact with DNA strongly. The emission from ethidium bromide (EB) bound DNA recorded in phosphate buffer solution (pH = 7.2) decreases by incremental addition of solution of the complexes. The complexes **4** and **5** (100 μM) bind with the minor groove of DNA and cleave double-stranded pBR322 DNA significantly even in the absence of an activator. In the presence of H$_2$O$_2$, they cleave supercoiled DNA via oxidative pathway even at lower concentration (20 μM). Both complexes **4** and **5** inhibit topoisomerase II activity with IC$_{50}$ values of 18 and 13. These values suggest that **4** and **5** are potential topoisomerase II inhibitors as compared to some of known inhibitors like novobiocin and etoposide.
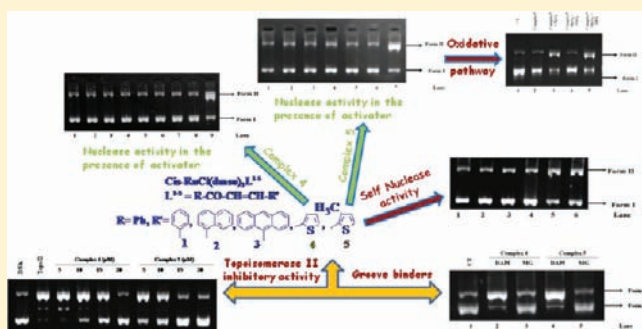
INTRODUCTION

The design and development of new anticancer drugs is an active area of research in chemical science. After the discovery of cisplatin by Rosenberg[1] as an effective anticancer drug having various side effects, the search for alternative metal based drugs has been an important area of interest for researchers. Among the several metals that are currently being investigated for their anticancer activity, ruthenium occupies a prominent position. In particular, *cis*-Ru(DMSO)$_4$Cl$_2$ is targeted as an antitumor drug[2] owing to its stabilization using heteroaromatic ligands[3] providing complexes like Na[trans-RuCl$_4$(S-DMSO)(Im)] (NAMI), [ImH][trans-RuCl$_4$(DMSO-S)Im] (NAMI-A), [IndH]trans-[Ru(N-Ind)$_2$Cl$_4$] (KP1019),[4] and Ru(η^6-p-cymene)Cl$_2$(pta) (RAPTA).[5] In this drug discovery approach, DNA has been targeted extensively as coordination of ruthenium atom to the nucleic bases is seen to get enhanced through H-bonding interactions or weakened because of steric interactions, suggesting the possibility to design compounds to target specific nucleotides. Ruthenium based antitumor complexes can interact with DNA by (1) electrostatic interaction between a cationic metal complex with DNA,[6] (2) noncovalent hydrophobic surface binding, (3) intercalation with DNA bases, and (4) covalent binding.[7−11] It is worth mentioning that labile ligands present in the coordination sphere of a ruthenium ion facilitate their substitution by DNA bases. The Ru(II) center bearing labile ligands binds double-helical DNA forming monofunctional adducts with DNA preferentially via N^7 atom of its guanine residues in a covalent binding mode.[12] The noncovalent interactions occur mainly through intercalation of aromatic skeleton and its binding with minor groove of DNA. Thus, DNA−drug intercalation could be stabilized significantly by π-electron overlap and hydrophobic and polar interactions as well as electrostatic forces of cationic intercalators with polyanionic nucleic acid.[13]

Since tumors maintain a high level of topoisomerase II (Topo II), inhibition of Topo II has also been considered as a target for the design of several antitumor agents.[14,15] The wide variety of topoisomerase inhibitors including etoposide, doxorubicin, mitoxantrone, amsacrine, and idarubicin kill cells undergoing DNA replication, reading the DNA for protein production or repair of DNA damage.[16] According to previous studies, Ru(II)(C$_6$H$_6$)(DMSO)Cl$_2$ exhibits a strong DNA-binding affinity and inhibits DNA relaxation activity of Topo II.[17] Thus, selection of synthetic precursor-like *cis*-Ru-(DMSO)$_4$Cl$_2$ which contains DMSO and chloro groups as labile ligands is justified. Additionally, chalcones being versatile

precursor for the synthesis of biologically relevant flavones also contributed to various biological properties.[18−24] Therefore, chalcones are considered as "privileged structure" by Evans et al.[25] as they bear bidentate (O,O) donor sites and could easily chelate with Ru(II) center substituting labile ligands. The chalcone bearing conjugated ligand frameworks may provide additional opportunity for their interaction with a DNA helix. Thus, presently synthesized and well characterized complexes were allowed to interact with calf thymus (CT) DNA, and their binding properties were monitored using UV−vis spectral titrations and competitive binding experiments. The DNA cleavage and topoisomerase inhibitory activities were monitored using gel electrophoretic mobility assay technique.

■ EXPERIMENTAL SECTION

Materials. The starting material *cis,fac*-[RuCl$_2$(DMSO-S)$_3$(DMSO-O)] was prepared from RuCl$_3$·3H$_2$O using a reported procedure.[26] However, different aldehydes, RuCl$_3$·3H$_2$O, 2-hydroxy acetophenone, and agarose were purchased from Sigma Aldrich Chemical Co. Pvt. Ltd., India. Solvents were purchased from E. Merck and used as received. Calf thymus (CT) DNA and supercoiled (SC) plasmid DNA pBR322 (as a solution in Tris buffer and cesium chloride purified), with a length of 4361 base pairs, were purchased from Bangalore Genei, India.

Instrumental Methods. Infrared, UV−vis, and luminescence spectra were recorded on VARIAN 3100 FTIR, Jasco UV-630 spectrophotometer and Perkin-Elmer LS-45 spectrophotometer, respectively. Elemental analysis and mass measurements were carried out using a Carbo-Erba elemental analyzer 1108 and JEOL SX-102 mass spectrometer, respectively. ¹H NMR spectra were recorded using JEOL AL 300 MHz spectrometer and TMS as internal reference.

Preparation of Chalcones. The chalcones, 1-(2-hydroxyphenyl)-3-(1-phenyl)propenone (L¹), 1-(2-hydroxyphenyl)-3-(1-naphathyl)-propenone (L²), 1-(2-hydroxyphenyl)-3-(9-anthracyl)propenone (L³), 1-(2-hydroxyphenyl)-3-(2-thienyl)propenone (L⁴), and 1-(2-Hydroxyphenyl)-3-(3-methyl-2-thienyl)-2-propen-1-one (L⁵), were synthesized and characterized using methods reported elsewhere.[27,28]

Synthesis of [Ru(L¹)(DMSO)$_3$Cl] (1). A solution of *cis,fac*-[RuCl$_2$(DMSO-S)$_3$(DMSO-O)] (484 mg, 1 mmol) dissolved in methanol (20 mL) was added dropwise to a methanolic solution (15 mL) of L¹ (224 mg, 1 mmol) containing an equimolar amount of NEt$_3$. After complete addition, the color of the resulting solution changed from orange to red, and stirring was continued for 12 h at room temperature. The red crystalline solid thus obtained was filtered and washed with methanol followed by diethyl ether and then dried in vacuo. Yield: 0.350 g (59%). Mp: >200 °C. The material is partially soluble in H$_2$O, ethanol, methanol, and tetrahydrofuran while it is highly soluble in acetone, dichloromethane, acetonitrile, DMSO, and chloroform. Anal. Calcd for C$_{21}$H$_{29}$O$_5$S$_3$ClRu Found (Calcd) (%): C 41.93 (42.45); H 4.69 (4.92). IR (KBr pellet, cm⁻¹): 2924(m) v(C—H), 1628(s) v(C=O), 1099 v(S=O), 425(m) v(Ru—S). ¹H NMR (CDCl$_3$, δ ppm): 7.76 (d, J = 8.4 Hz, 1H, Ar), 7.61 (m, 4H, Ar and H$_\alpha$), 7.43 (m, 4H, Ar and H$_\beta$), 7.32 (m, 1H, Ar), 6.96 (d, J = 8.4 Hz, 1H, Ar), 6.58 (t, J = 7.5 Hz, 1H, Ar) 3.56−3.09 (s and m, 18H, DMSO). ¹³C NMR (CDCl$_3$, δ ppm): 188.89 (C=O), 171.64 (Ar—CO), 143.57 (C-α), 121.70 (C-β), 136.6, 134.91, 132.21, 130.58, 129.05, 128.24, 125.60, 124.31, 115.22 (Ar), 47.38, 46.61, 45.84, 44.64, 44.24, 42.87 (CH$_3$, DMSO). UV−vis (DMF, 10⁻⁴ M): λ_{max} (nm) (ε_{max} × 10⁴ M⁻¹ cm⁻¹) 239 (1.51), 329(1.45), 494 sh (0.273).

Other complexes were also prepared adopting the procedure similar to that used for the preparation of complex **1** using L², L³, L⁴, L⁵ separately in place of L¹.

Complex [Ru(L²)(DMSO)$_3$Cl] (2). Yield: 0.388 g (60%). Mp: >200 °C. Anal. Calcd for C$_{25}$H$_{31}$O$_5$S$_3$ClRu (**2**) Found (Calcd) (%): C 46.41 (46.61); H 4.78 (4.85). IR (KBr pellet, cm⁻¹): 2922(m) v(C—H), 1616(s) v(C=O), 1100(s) v(S=O), 428(m) v(Ru—S). ¹H NMR (CDCl$_3$, δ ppm): 8.4 (d, J = 15 Hz, 1H, H$_\alpha$), 8.093 (d, J = 7.8 Hz, 1H, Ar), 7.89 (m, 4H, Ar), 7.74 (d, J = 15 Hz, 1H, H$_\beta$), 7.59 (m, 3H, Ar),

7.33 (m, 1H, Ar), 6.98 (d, J = 8.4 Hz, 1H, Ar), 6.59 (t, J = 7.5 Hz, 1H, Ar), 3.62−3.15 (s and m, 18H, DMSO). ¹³C NMR (CDCl$_3$, δ ppm): 188.53 (C=O), 171.71 (Ar−CO), 140.48 (C-α), 121.66 (C-β), 136.66, 133.70, 132.38, 132.22, 131.48, 130.89, 128.95, 127.23, 126.66, 126.35, 125.62, 125.54, 125.23, 122.88, 115.30, (Ar), 47.40, 46.63, 45.95, 44.59, 44.19, 42.91 (CH$_3$, DMSO). UV−vis (DMSO, 10⁻⁴ M): λ_{max} (nm) (ε_{max} × 10⁴ M⁻¹ cm⁻¹) 271 (1.10), 370 (0.996), 495 sh (0.193).

Complex [Ru(L³)(DMSO)$_3$Cl] (3). Yield: 0.400 g (58%). Mp: >200 °C. Anal. Calcd for C$_{29}$H$_{33}$O$_5$S$_3$ClRu Found (Calcd) (%): C 50.14 (50.17); H 4.74 (4.79). ESI-MS: m/z: 694 [M]⁺, 659 [M − Cl]⁺, 581 [M − Cl − DMSO]⁺, 503 [M − Cl − 2DMSO]⁺, 425 [M − Cl − 3DMSO]⁺. IR (KBr pellet, cm⁻¹): 3006(m) v(C−H), 1612(s) v(C=O), 1107(s) v(S=O), 426(m) v(Ru−S). ¹H NMR (CDCl$_3$, δ ppm): 8.58 (m, 2H, H$_\alpha$ and Ar), 8.27 (d, J = 7.8 Hz, 1H, Ar), 8.05 (d, J = 7.2 Hz, 1H, Ar), 7.72 (m, 6H, Ar and H$_\beta$), 7.33 (m, 1H, Ar), 7.02 (d, J = 8.7 Hz, 1H, Ar), 6.53 (t, J = 7.5 Hz, 1H, Ar), 3.64−3.19 (s and m, 18H, DMSO). ¹³C NMR (CDCl$_3$, δ ppm): 188.29 (C=O), 171.87 (Ar−CO), 140.41 (C-α), 121.55 (C-β), 136.75, 133.07, 132.33, 131.27, 129.90, 129.56, 129.00, 128.72, 126.76, 125.63, 125.49, 125.03, 115.35 (Ar), 47.54, 46.65, 46.35, 44.76, 44.12, 42.90 (CH$_3$, DMSO). UV−vis (DMSO, 10⁻⁴ M): λ_{max} (nm) (ε_{max} × 10⁴ M⁻¹ cm⁻¹) 357(0.647), 444 (1.089), 516(0.037).

Complex [Ru(L⁴)(DMSO)$_3$Cl] (4). Yield: 0.400 g (67%). Mp: >200 °C. Anal. Calcd for C$_{19}$H$_{27}$O$_5$S$_4$ClRu Found (Calcd) (%): 37.56 (38.02); H 4.74 (4.53). IR (KBr pellet, cm⁻¹): 3010(m) v(C−H), 1613(s) v(C=O), 1098(s) v(S=O), 427(m) v(Ru−S). ¹H NMR (CDCl$_3$, δ ppm): 7.73 (m, 2H, thiophene and H$_\alpha$), 7.45 (m, 2H, Ar and thiophene), 7.30 (m, 2H, H$_\beta$ and thiophene), 7.1 (m, 1H, Ar), 6.94 (d, J = 8.7 Hz, 1H, Ar), 6.59 (t, J = 7.5 Hz, 1H, Ar), 3.55−3.09 (s and m, 18H, DMSO). ¹³C NMR (CDCl$_3$, δ ppm): 187.98 (C=O), 171.57 (Ar−CO), 140.51 (C-α), 121.78 (C-β), 136.52, 128.44, 122.93 (thiophene), 136.11, 131.77, 129.14, 125.55, 115.28 (Ar), 42.95, 44.28, 44.65, 45.69, 46.58, 47.38 (CH$_3$, DMSO). UV−vis (DMSO, 10⁻⁴ M): λ_{max} (nm) (ε_{max} × 10⁴ M⁻¹ cm⁻¹) 291 (0.49), 368 (1.22), 501 (0.23).

Complex [Ru(L⁵)(DMSO)$_3$Cl] (5). Yield: 0.370 g (56%). Mp: >200 °C. Anal. Calcd for C$_{20}$H$_{29}$O$_5$S$_4$ClRu (%): C 39.26 (39.11); H 3.92 (4.76) %. IR (KBr pellet, cm⁻¹): 3091(m) v(C−H), 1612(s) v(C=O), 1102(s) v(S=O), 424(m) v(Ru−S). ¹H NMR (CDCl$_3$, δ ppm): 7.87 (d, J = 15 Hz, 1H, H$_\alpha$), 7.73 (d, J = 8.4 Hz, 1H, Ar), 7.38 (m, 3H, Ar, H$_\beta$ and thiophene), 6.94 (m, 2H, Ar and thiophene), 6.59 (t, J = 7.5 Hz, 1H, Ar), 3.56−3.08 (s and m, 18H, DMSO), 2.34 (s, 3H, CH$_3$). ¹³C NMR (CDCl$_3$, δ ppm): 187.98 (C=O), 171.50 (Ar−CO), 142.27 (C-α), 121.54 (C-β), 131.44, 131.82, 136.38 (thiophene), 134.92, 134.77, 127.88, 125.52, 115.26 (Ar), 47.36, 46.61, 44.55, 44.29, 43.06 (CH$_3$, DMSO), 14.30 (CH$_3$). UV−vis (DMSO, 10⁻⁴ M): λ_{max} (nm) (ε_{max} × 10⁴ M⁻¹ cm⁻¹) 292 (0.51), 374 (1.54), 504 (0.37).

X-ray Crystallographic Studies. Crystals of complexes suitable for X-ray diffraction were grown at room temperature in a mixture of dichloromethane/petroleum ether (40−60 °C) solvent. The X-ray crystallographic data were recorded by mounting single-crystal of the complexes separately on a glass fiber. Oxford diffraction XCALIBUR-S CCD area detector diffractometer was used for the determination of cell and intensity data collection. Appropriate empirical absorption corrections were applied using multiscan programs. Monochromated Mo Kα radiation (λ = 0.710 73 Å) was used for the measurements. The crystal structures were solved by direct methods and refined by full-matrix least-squares SHELXL-97,[29] and special computations were carried out using PLATON.[30]

Electrochemical Studies. Cyclic voltammetry was performed on a CHI 620c electrochemical analyzer. A glassy carbon working electrode, platinum wire auxiliary electrode, and Ag/Ag⁺ reference electrode were used in a standard three-electrode configuration. Tetrabutylammonium perchlorate (TBAP) was used as a supporting electrolyte, and the solution concentration was kept as 10⁻³ M.

Absorption Titration. The experiments of DNA binding with complexes were carried out in Na-phosphate buffer solution (pH 7.2). The absorption ratio of CT DNA solutions at λ_{max} 260 and 280 nm was found as 1.9:1. It showed that DNA is sufficiently free from

protein impurities. The concentration of DNA was determined using UV–vis absorbance and the molar absorption coefficient (6600 M^{-1} cm^{-1}) at 260 nm.[31] The absorption titrations of the complexes (10 μM in Na-phosphate buffer containing 0.01% DMSO) against CT DNA were performed by monitoring their absorption spectra with incremental addition of CT DNA within 1–10 μM concentration. The spectra were recorded after equilibration for 3 min, allowing the complexes to bind to the CT-DNA. The intrinsic binding constant (K_b) was calculated from a plot of $[DNA]/(\varepsilon_a - \varepsilon_f)$ versus $[DNA]$ using the following equation:

$$[DNA]/(\varepsilon_a - \varepsilon_f) = [DNA]/(\varepsilon_b - \varepsilon_f) + [K_b(\varepsilon_b - \varepsilon_f)]^{-1} \quad (1)$$

$[DNA]$ is the concentration of DNA in base pairs. The apparent absorption coefficients ε_a, ε_f, and ε_b correspond to $A_{obsd}/[Ru]$, the extinction coefficient for free ruthenium(II) complexes and extinction coefficient for the ruthenium(II) complex in fully bound form, respectively.[32] The value of K_b was calculated as the ratio of the slope to the intercept.

Competitive Binding with Ethidium Bromide. Relative binding of ruthenium complexes with CT DNA was studied by fluorescence spectral method using bound CT DNA solution in Na phosphate buffer solution (pH 7.2). In a typical experiment, 20 μL of CT-DNA solution (A_{260} = 2.0) was added to 2 mL of ethidium bromide (EB) in buffer solution, and the fluorescence intensity was measured at excitation wavelength λ, 510 nm; maximum emission was observed at λ, 600 nm. Aliquots of 0.1 mM solution of the complexes were then added to DNA-EB, and resulting fluorescence spectra were recorded after each addition until maximum reduction in the intensity of fluorescence occurred. The Stern–Volmer quenching constant[33] in each complex was calculated using the equation given as

$$I_o/I = 1 + K_{sv}r \quad (2)$$

Here, I_o and I are the fluorescence intensity in the absence and presence of complexes, respectively, K_{sv} is a linear Stern–Volmer quenching constant, and r is the ratio of the total concentration of a complex to that of DNA. The value of K_{sv} is given by the ratio of slope to intercept in a plot of I_o/I versus $[complex]/[DNA]$.

DNA Cleavage Studies Using Agarose Gel Electrophoresis. In the gel electrophoresis experiments, supercoiled pBR322 DNA was treated with metal complexes, and the mixture was incubated for 30 min at 37 °C. The samples were then analyzed by 1.5% agarose gel electrophoresis [Tris–acetic acid–ethylenediaminetetraacetic acid (EDTA) (TAE) buffer, pH 8.3] for 3 h at 50 mV. The gel was stained with 0.5 μg mL^{-1} ethidium bromide, visualized by UV light, and photographed for analysis. The extent of cleavage of the SC DNA was determined by measuring the intensities of the bands using Alpha Innotech gel documentation system (AlphaImager 2200)and Gen-osens 1510 documentation and analysis system. The experiments were also carried out in the presence of activators, viz., NaN_3 (^1O singlet oxygen trapper), sodium formate (OH^- radical scavanger), sodium ascobate (reducing agent), and H_2O_2, which were added to SC DNA prior to the addition of complexes **4** and **5** (acetonitrile 0.01%) only.

Topoisomerase Inhibition Assay. DNA topoisomerase II (Topo II) from *Escherichia coli* was purchased from New England Biolabs, and no further purification was performed. One unit (U) of the enzyme was defined as the amount that completely relaxed 0.5 μg of negatively charged supercoiled pBR322 plasmid DNA in 30 min at 30 °C under standard assay conditions. The reaction mixture (20 μL) consists of 35 mM Tris–HCl (pH 7.5), 24 mM KCl, 4.0 mM $MgCl_2$, 2 mM DTT (dithiothreitol), 5 mM spermidine, 0.1 mg/mL BSA, 1.75 mM ATP, 6.5% glycerol, 0.30 μg of pBR322 DNA, and 1 U of Topo II together with variable concentration of Ru(II) complexes (0–20 μM). The corresponding reaction mixtures were incubated at 37 °C for 30 min, and then they were terminated by the addition of 3 μL of 5× stop solution dye consisting of 0.25% bromophenol blue, 4.5% sodium dodecyl sulfate, and 45% glycerol. The electrophoresis of the samples was carried out through 1% agarose in TAE buffer at 50 V for 2 h. The gel was stained with 1 μg mL^{-1} EB and photographed under UV light. The concentration of the inhibitor that prevented 50% of the

supercoiled DNA from being converted into relaxed DNA (IC_{50} values) was calculated from the midpoint concentration of the complex-induced DNA unwinding. To check whether the order of addition affected the results, experiments were also carried out in ice, in which the whole reaction mixture was assembled.

■ RESULTS

Description of Molecular Structure. The complexes (Scheme 1) were found to be air stable both in solid as well as

Scheme 1. Schematic Representation of Synthetic Strategy
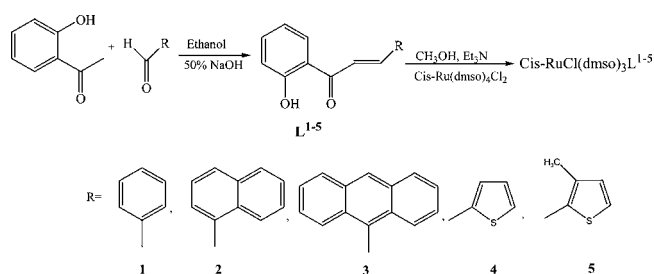
in solution. The molecular structures along with crystallographic numbering schemes of complexes are illustrated in Figure 1a–e. Crystallographic data and selected bond distance/bond angle data are shown in Table 1 and Supporting Information, respectively. The complexes **1**, **2**, and **4** crystallized as block-shaped crystals in a triclinic crystal system with space group $P\bar{1}$ while complexes **3** and **5** crystallized in monoclinic crystal system with space group $P2_1/c$ and $C2/c$, respectively. All the complexes exhibited distorted octahedral geometry around the metal center as expected from low spin d^6 Ru(II) ion. No solvent accessible voids could be seen from the packing pattern of the complexes **1**, **2**, **3**, and **4**, while in complex **5** dichloromethane and water molecules were present. The $S(2)-O(3)$ bond distances [1.47(5), 1.48(18), 1.46(4),1.48(5), 1.49(7) Å] in complexes were found to be comparable with that observed in free DMSO [1.49(1) Å].[34] The chalcone exists in bis chelating coordination mode (η^2), and chelating angles were found as 88.20(15)°, 88.25(5)°, 88.72(14)°, 88.30(16)°, and 88.80(3)° in the molecular structure of complexes **1**, **2**, **3**, **4**, and **5**, respectively.

The bond lengths (Ru–O, Ru–S, and Ru–Cl) vary in the order (Ru–Cl) > (Ru–S) > (Ru–O).[27] The C1–O1–Ru1–O2-C7 atoms lie in the same plane. The $O(1)-Ru(1)-S(2)$ angles in all complexes were found to be significantly smaller than 180°; it may be due to steric repulsion of the methyl group of DMSO and phenyl ring of the chalcone. The two oxygen atoms of the ligand are bonded to the Ru(II) center, and the $Ru(1)-O(1)$ distance varies from 2.0514(17) to 2.091(4) Å whereas the $Ru(1)-O(2)$ distance varied from 2.055(4) to 2.0726(17) Å and was found to be consistent with the reported values.[35] Additionally, Ru–S distance varied from 2.246(10) to 2.266(9) Å, and Ru–Cl bond length was found from 2.407(3) to 2.418 (15) Å. Probably this longer distance for Ru–Cl as compared to the Ru–S bond made fast substitution of Cl by nucleobases.

The molecular structures of the complexes obtained from their X-ray diffraction studies were supported by their spectroscopic measurements in the solution. The IR spectra of the chalcones in general display characteristic peaks at 3446–3458 and 1638–1689 cm^{-1} assigned to $v(OH)$ and $v(C=O)$ vibration, respectively, and were found to be
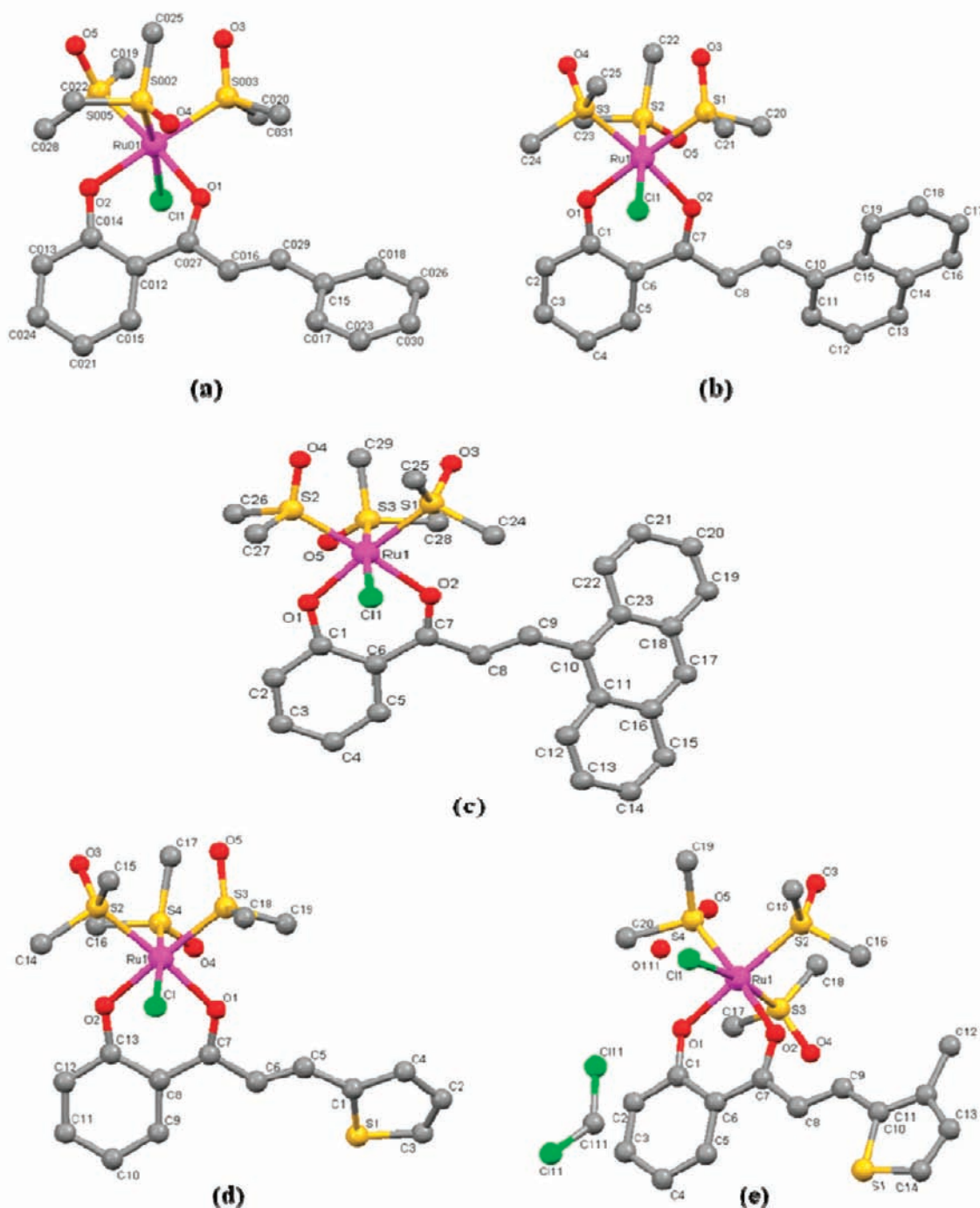
Figure 1. Molecular structure of (a) complex **1**, (b) complex **2**, (c) complex **3**, (d) complex **4**, (e) complex **5**. Hydrogen atoms are omitted for clarity.

consistent with the earlier report.[27,28] As compared to the spectra of free ligands, the IR spectra of their complexes displayed peaks at 1628, 1615, 1612, 1617, and 1616 cm^{-1}, respectively, and supported the coordination of their $v(C=O)$ group. Since the $v(O-H)$ vibration of free ligands disappeared in the spectra of their corresponding complexes, it is considered that the deprotonated OH group has coordinated with the metal ion. Additional peaks observed at 1100−1050 and 425−430 cm^{-1} are assigned to $v(S=O)$ and $v(Ru-S)$ vibrations.

^{1}H and ^{13}C NMR spectral data of the complexes are incorporated in the Experimental Section and Supporting Information. The OH proton observed in the spectra of free

chalcones disappeared in the spectra of corresponding complexes, again supporting the deprotonation of the OH group. An appreciable downfield shift of ethylenic protons was also observed as a consequence of the coordination of neighboring C=O group. Since there is no peak observed for O-bonded DMSO at δ ~2.72 ppm, all DMSO is assigned to be S-coordinated to the metal center. In ^{13}C NMR spectra, C=O carbon of the chalcones in the complexes appeared at δ 187.98−188.89 ppm while the O−C−Ar carbon atoms of chalcones appeared at δ 171.49−171.90 ppm. The carbon atoms of phenyl groups as well as methyl groups of DMSO

Table 1. Selected Crystallographic Data of Complexes 1, 2, 3, 4, and 5^a

	1	2	3	4	5
formula	$C_{21}H_{29}O_5S_3ClRu$	$C_{25}H_{31}O_5S_3ClRu$	$C_{29}H_{33}O_5S_3ClRu$	$C_{19}H_{27}O_5S_4ClRu$	$C_{41}H_{58}O_{12}S_8Cl_4Ru_2$
M	594.17	644.20	694.25	600.17	1343.37
cryst syst	triclinic	triclinic	monoclinic	triclinic	monoclinic
T (K)	150(2)	293(2)	150(2)	293(2)	150(2)
space group	$P\bar{1}$	$P\bar{1}$	$P2_1/c$	$P\bar{1}$	$C2/c$
a/Å	8.3200(4)	8.3503(3)	8.3752(3)	8.2466(4)	23.2656(17)
b/Å	12.4615(9)	12.0760(7)	24.7738(9)	12.3466(7)	11.7850(5)
c/Å	12.9858(10)	13.9832(6)	14.2933(6)	12.9838(7)	23.5597(18)
α (deg)	107.394(7)	73.436(4)	90	106.590(5)	90
β (deg)	103.270(5)	83.884(3)	95.429(4)	101.295(4)	120.357(10)
γ (deg)	94.901(5)	88.764(4)	90	95.912(4)	90
V/ Å^3	1233.17(14)	1343.78(11)	2952.3(2)	1224.52(11)	5574.0(6)
Z	2	2	4	2	4
D_c/mg m^{-3}	1.600	1.592	1.562	1.628	1.601
reflns collected/unique	7811/5293	8822/5709	22 306/5164	9084/5381	19 642/4897
data/restraints/params	5293/0/280	5709/0/316	5164/0/358	5381/0/128	4897/0/310
R(int)	0.0331	0.0189	0.0906	0.0199	0.0738
θ range for data collection (deg)	2.91−25.00	2.91−25.00	3.29−25.00	2.91−25.00	3.46- 25.00
completeness to θ = 25.00	98	99.4	99.8	98	99.8
wR2	0.1762	0.0734	0.0841	0.2190	0.2509
R1	0.0614	0.0295	0.0432	0.0680	0.0974
GOF	1.105	0.738	0.809	1.012	1.221
largest diff. peak and hole (e Å^{-3})	2.277 and −2.320	1.100 and −0.347	1.004 and −0.375	2.888 and −2.563	4.354 and −1.592

^{a}Refinement method: full-matrix, least-squares on F^2.

appeared in the ranges δ 115.22−136.75 and δ 40.98−47.66 ppm, respectively.

The ESI-MS of a representative complex **3** was also recorded to support the stability of complexes in the solution. It showed molecular ion peak at m/z 694 assigned to $[M]^+$. However, additional peaks observed at 659, 581, 503, and 425 were assigned to $[M − Cl]^+$, $[M − Cl − DMSO]^+$, $[M − Cl − 2DMSO]^+$, $[M − Cl − 3DMSO]^+$, respectively.

In the electronic spectra of complexes, the intense bands observed at higher energy showed greater dependence on the nature of the O,O-ligands. The remaining less intense bands were attributed to charge transfer transitions from chlorides to Ru(II) ion. The low spin ruthenium(II) ion (d^6 configuration) provides filled metal orbitals of proper symmetry and interacts with relatively low lying π* orbitals of the ligand. The broad bands observed at λ_{max} 494−516 nm arise from dπ(Ru^{II})→ π*(L$^{1−5}$) metal-to-ligand charge-transfer (MLCT) transitions. It is reported that substitution by a more conjugated ligand enhances π-delocalization and hence lowers the energy between dπ(Ru^{II})→π*(ligand) MLCT band.[36] So an attempt was made to correlate such variation in complexes **1**, **2**, and **3**. The higher energy bands observed at 230−375 nm in the spectra of the complexes are assigned to intraligand and π−π* transitions. These bands were red-shifted as compared to the band observed from respective ligands. The spectral features of the complexes are shown Figure 2.

Cyclic Voltammetry. Cyclic voltammetry of complexes was carried out in dichloromethane at 298 K using ferrocene/ ferrocenium (Fc/Fc$^+$) as an internal standard (0.10 V (80 mv) vs Ag/Ag$^+$). The mixed-ligand complexes showed irreversible oxidation peak from 0.79 to 0.93 V assigned to Ru^{III}/Ru^{II} redox couple;[37] the data are summarized in Table 3, and figures are shown as Supporting Information. This irreversibility could be considered in view of the transient lifetime of the reduced state as reported earlier.[38] However, the lower value of oxidation
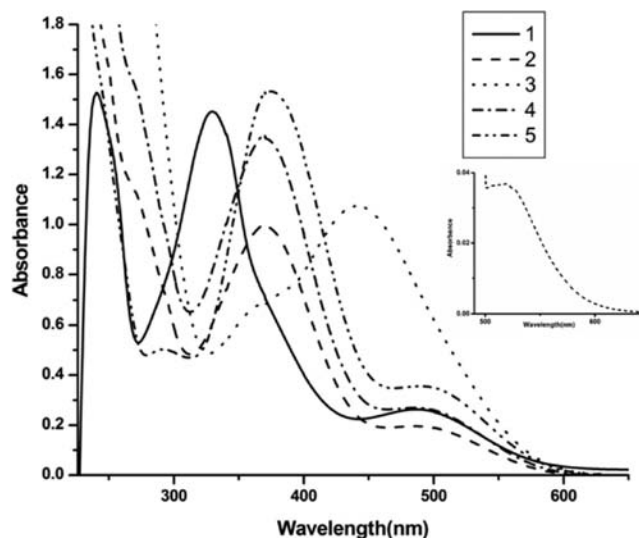

Figure 2. Overlay UV−vis spectra of complexes **1−5** recorded in dichloromethane (1×10^{-4} M). Inset: MLCT region of the complex **3**.

potential for Ru(III)/Ru(II) couple in complex **1** could be attributed to the stronger σ-donor and weaker π-acceptor ability of the ligands, consequently stabilizing the higher oxidation state of Ru(III).[39] The oxidation potential data suggested that metal based oxidation varied in order of $E_{1/2}(3)$ < $E_{1/2}(5)$ < $E_{1/2}(4)$ < $E_{1/2}(2)$ < $E_{1/2}(1)$. This order goes with the order of their MLCT transition energies. The lower value of $E_{1/2}$ for the oxidation of Ru(II) to Ru(III) found in complex **5** as compared to its value in complex **4** could be considered due to the presence of electron repelling the methyl group in the thiophene ring of ligand.[40]

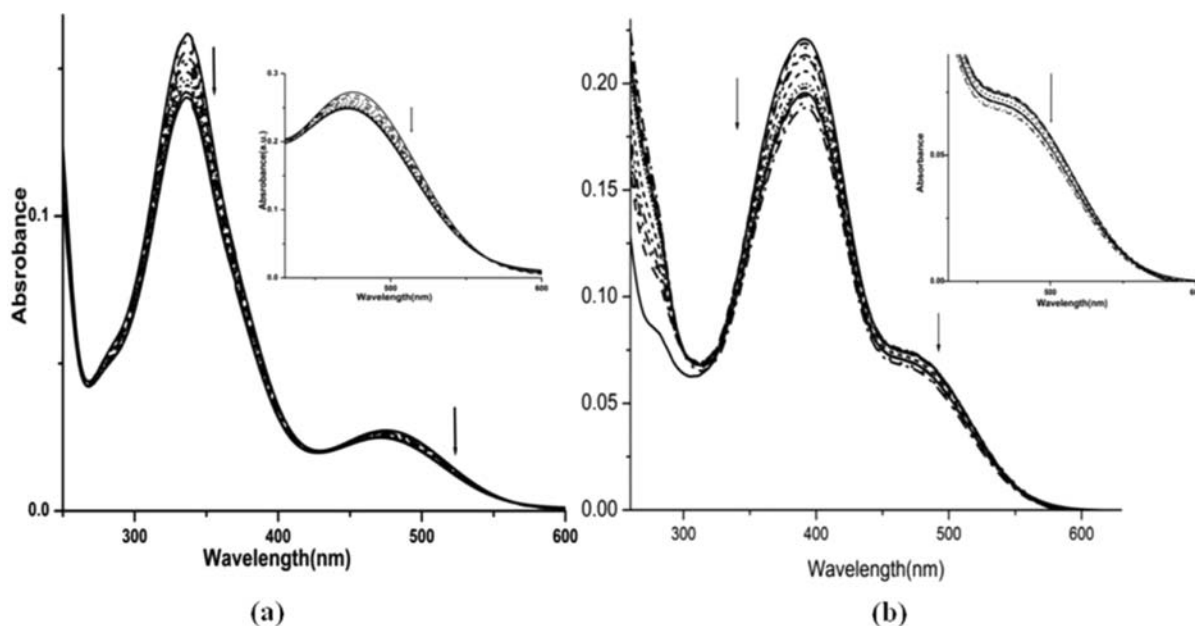**DNA Interaction.** Electronic absorption spectroscopy is found to be an effective tool to examine the binding mode of

Figure 3. UV−vis absorption spectra of (a) complex **1** (10 μM) in the absence and in the presence of increasing amounts of DNA = 0−100 μM and (b) complex **5** (10 μM) in the absence and in the presence of increasing amounts of DNA = 0−100 μM. Arrow shows the absorbance changes upon increasing DNA concentration.

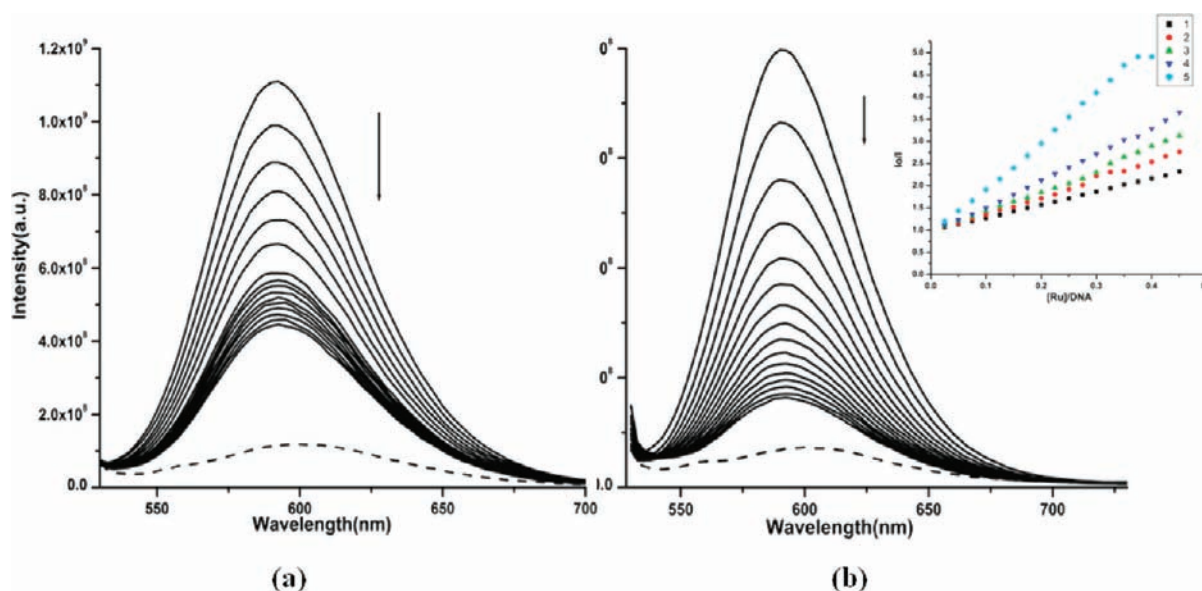**Figure 4.** Emission spectra from EB bound DNA in the absence (---) and in the presence of [complex **1** and **5**] 0−4 μM concentration, [EB] 10 μM, [DNA] 10 μM. Arrow shows changes in the emission intensity upon addition of increasing concentration of the complex. Inset: Plots of I_o/I vs [Ru]/[DNA] with experimental data points.

DNA with metal complexes.[41] Thus, to explore the possibility of binding of each complex to CT-DNA, spectroscopic titrations of the solution of complexes separately with CT-DNA were carried out. The ruthenium(II) complexes can bind to double-stranded DNA in different binding modes on the basis of their structure, charge, and type of ligands. In order to compare the binding strength of the complexes with CT DNA, the intrinsic binding constant K_b was calculated by monitoring the changes in their absorbance with increasing concentration of DNA (Figure 3). The value of K_b was obtained as a ratio of slope to intercept obtained from the plot of $[DNA]/(\varepsilon_a - \varepsilon_f)$ versus [DNA]. The K_b values were obtained as 4.22×10^5, 5.29×10^5, 7.09×10^5, 4.9×10^6, and 5.7×10^6 for complexes **1**, **2**,

3, **4**, and **5**, respectively. The K_b values thus vary in the order K_b (**5**) > K_b (**4**) > K_b (**3**) > K_b (**2**) > K_b (**1**).

Competitive Binding of Complexes with Ethidium Bromide. Ethidium bromide (EB) is a standard intercalating agent of DNA. Hence, a competitive binding study using ethidium bromide (EB) bound to DNA was carried out by successive addition of 0−0.25 μM of each complex to 10 μM DNA solutions containing 10 μM solution of EB in Na-phosphate buffer (pH 7.2). The emission spectra of EB-DNA system in the presence and absence of ruthenium complexes **1** and **5** are shown in Figure 4. The plots of I_o/I versus [complex]/[DNA] are shown in Figure 4. They support the linear Stern−Volmer equation. The Stern−Volmer constant
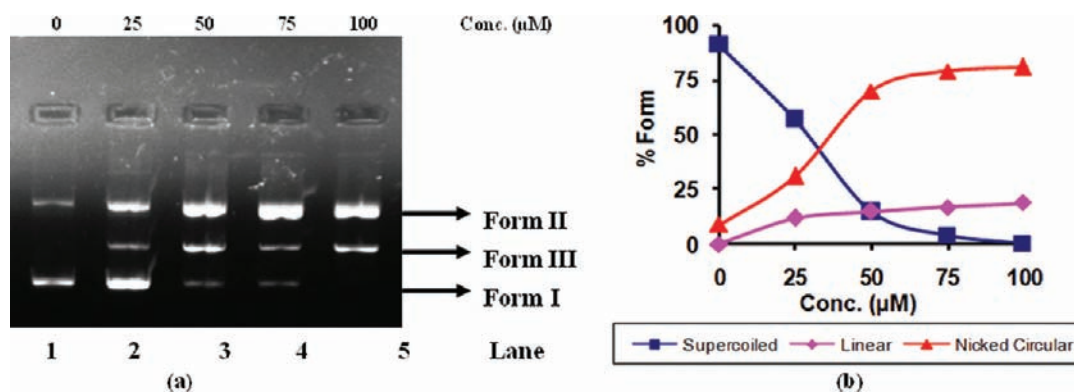
Figure 5. (a) Ethidium bromide stained agarose gel (1%) of pBR322 plasmid DNA (300 ng μL^{-1}) in the presence of complex **4** after 1 h of incubation: lane 1, DNA control; lane 2, pBR322 + 25 μM; lane 3, pBR322 + 50 μM; lane 4, pBR322 + 75 μM; lane 5, pBR322 + 100 μM. (b) Cleavage of supercoiled pBR322 DNA showing the decrease in SC DNA and the formation of NC DNA with increasing concentration of complex **4**.
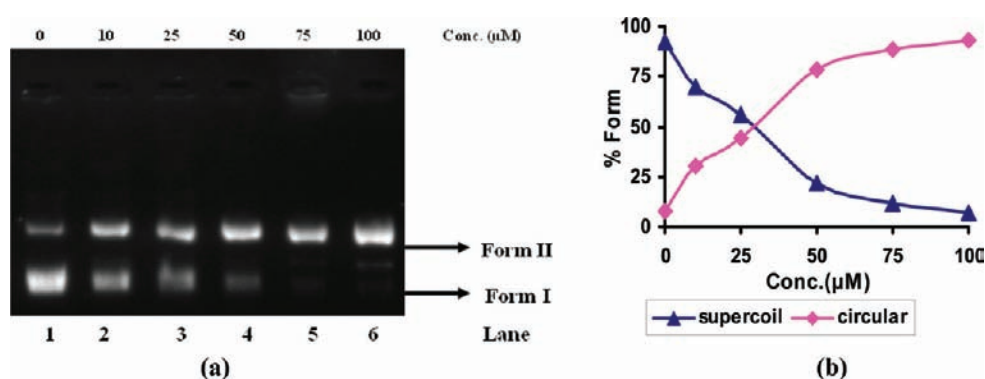

Figure 6. (a) Ethidium bromide stained agarose gel (1%) of pBR322 plasmid DNA (300 ng μL^{-1}) in the presence of complex **5** after 1 h of incubation: lane 1, DNA control; lane 2, pBR322 + 10 μM; lane 3, pBR322 + 25 μM; lane 4, pBR322 + 50 μM; lane 5, pBR322 + 75 μM; lane 6, pBR322 + 100 μM. (b) Cleavage of supercoiled pBR322 DNA showing the decrease in SC DNA and the formation of NC DNA with increasing concentration of complex **5**.
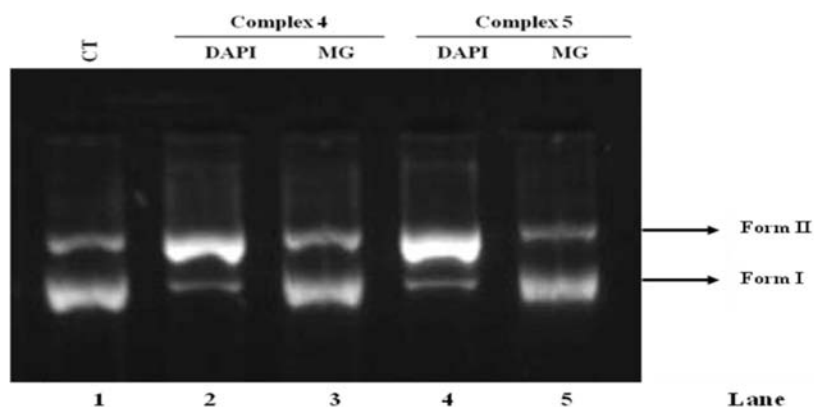

Figure 7. Ethidium bromide stained agarose gel (1%) of pBR322 plasmid DNA (300 ng μL^{-1}) in the presence of 20 μM complexes after 1 h of incubation: lane 1, DNA control; lane 2, pBR322 + **4** + DAPI; lane 3, pBR322 + **4** + MG; lane 4, pBR322 + **5** + DAPI; lane 5, pBR322 + **5** + MG.

(K_{sv}) is evaluated as 5.3, 4.2, 3.8, 1.8, and 1.2 for complexes **5**, **4**, **3**, **2**, and **1**, respectively, which were in parity with the extent of displacement of ethidium bromide by the complexes. The hydrogen bond may be formed between the sulfur of the thiophene group, present in the ligand of the complexes **4** and **5**, and the complementary functional group present on the edge of the DNA.[42]

Nuclease Activity of the Complexes in the Absence of Activators. To assess the DNA cleavage ability of the complexes, supercoiled pBR322 DNA (300 ng μL^{-1}) was

incubated separately with 100 μM of all complexes in 5 mM Tris-HCl/50 mM NaCl buffer at pH 7.2 for 1 h without addition of any activator as depicted in the Supporting Information. Control experiment showed that SC DNA (form I) was cleaved only by complexes **4** and **5**, and formed NC DNA (form II). However, a preliminary experiment showed that L^1–L^5 separately did not cause any cleavage (Supporting Information) of DNA at 100 μM concentration.

In order to study DNA cleavage pattern of complexes **4** and **5**, different concentrations (0–100 μM) of **4** and **5** were
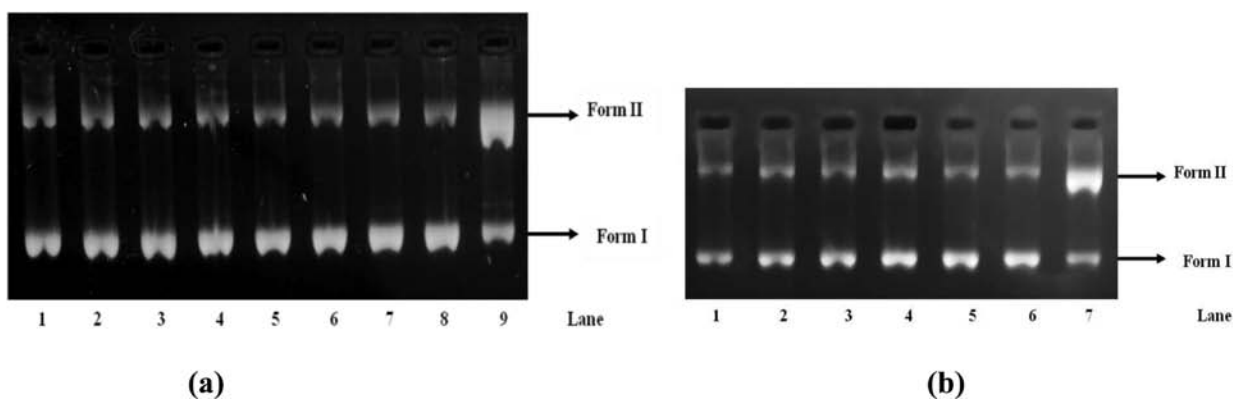
Figure 8. (a) Ethidium bromide stained agarose gel (1.5%) of pBR322 plasmid DNA (300 ng μL^{-1}) in the presence of complex **4** (20 μM) after 1 h of incubation: lane 1, DNA control; lane 2, DNA + NaN$_3$ (50 μM); lane 3, DNA + NaN$_3$ (50 μM) + **4**; lane 4, DNA + sodium formate (50 μM); lane 5, DNA + sodium formate (50 μM) + **4**; lane 6, DNA + sodium ascorbate; lane 7, DNA + sodium ascorbate + **4**; lane 8, DNA + H$_2$O$_2$ (50 μM); lane 9, DNA + H$_2$O$_2$ (50 μM) + **4**. (b) Ethidium bromide stained agarose gel (1.5%) of pBR322 plasmid DNA (300 ng μL^{-1}) in the presence of complex **5** (20 μM) after 1 h of incubation: lane 1, DNA control; lane 2, DNA + NaN$_3$ (50 μM); lane 3, DNA + NaN$_3$ (50 μM) + **5**; lane 4, DNA + sodium formate (50 μM); lane 5, DNA + sodium formate (50 μM) + **5**; lane 6, DNA + H$_2$O$_2$ (50 μM); lane 7, DNA + H$_2$O$_2$ (50 μM) + **5**.

incubated with pBR322 DNA for 1 h separately in 15 μL of the two separate reaction mixtures. Both complexes caused a linear increase in the intensity of NC DNA band accompanied with the similar decline in SC DNA in a concentration dependent manner in aqueous buffer solution. Complexes **4** and **5** both converted more than 90% of SC form into NC form at a concentration of 100 μM. Complex **4** was generated into both nicked circular and linear forms from its SC form at a concentration of 100 μM as depicted in Figure 5 while 100 μM of **5** completely converted into nicked circular form as shown in Figure 6. DNA cleavage by complex **5** is significantly higher than that observed with complex **4**, which could be related to the presence of the electron releasing methyl group as substituent.

DNA Cleavage in Presence of Minor and Major Groove Binding Agents. The potential interacting site of the complex with supercoiled plasmid pBR322 DNA was performed by recognition elements, minor groove binding agent 4′,6-diamidino-2-phenylindole (DAPI) and major groove binding agent, methyl green (MG).[43] The supercoiled DNA was treated separately with DAPI and MG prior to the addition of the complexes **4** and **5**. The degree of binding of the complex with pBR322 DNA in the presence of DAPI and MG is found as 79% and 21% in complex **4** and 86% and 24% in complex **5**, respectively (Figure 7).

Investigation of DNA Cleavage in Presence of Activator and Radical Scavengers. The involvement of reactive oxygen species (hydroxyl, singlet oxygen, and hydrogen peroxide) in the nuclease mechanism could be inferred by monitoring the quenching of DNA cleavage in the presence of radical scavengers[44] in the solution. Complexes **1**, **2**, and **3** did not cleave DNA in the presence of scavengers like NaN$_3$ (^{1}O singlet oxygen trapper), sodium formate (OH$^\bullet$ radical scavenger), and H$_2$O$_2$ (both oxidizing agent as well as reducing agent). However, complexes **4** and **5** in the presence of H$_2$O$_2$ converted from I form to II form of DNA even at lower concentration (20 μM) as depicted in Figure 8a,b. It is further supported by the experiment using a representative complex **5** as depicted in Figure 9 (lane 4) that H$_2$O$_2$ in the presence of NaN$_3$ is unable to assist the cleavage of DNA. It is perhaps due to trapping of O$_2$ (H$_2$O$_2$ → H$_2$O + O$_2$) by NaN$_3$, hence inhibiting the oxidation of DNA bases, especially guanine.

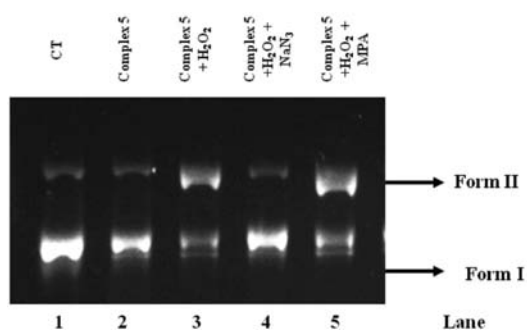**Figure 9.** Ethidium bromide stained agarose gel (1%) of pBR322 plasmid DNA (300 ng μL^{-1}) in the presence of complex **5** (20 μM) after 1 h of incubation: lane 1, DNA control; lane 2, DNA + **5**; lane 3, DNA + H$_2$O$_2$ (50 μM) + **5**; lane 4, DNA + H$_2$O$_2$ (50 μM) + sodium azide (50 μM); lane 5, DNA + H$_2$O$_2$ (50 μM) + 3-mercaptopropionic acid (50 μM) + **5**.

Thus, H$_2$O$_2$ induced DNA cleavage in the presence of complexes **4** and **5** following an oxidative pathway.

Topoisomerase Inhibition Assay by the Ruthenium Complexes. Topoisomerase inhibitory reactions were performed by complexes **4** and **5**. Complex **5** completely inhibited Topo II without promoting the formation of linear DNA products, and similar results were also observed with complex **4** as depicted in Figure 10. Both Ru(II) complexes inhibited the activity of Topo II at a low concentration (IC$_{50}$ < 20 μM), comparable to some classical Topo II inhibitors as shown in Table 2. Similar to that described before for Topo II, the DNA strand passage assay was also used to distinguish the effects of Ru(II) complexes on Topo II function from their effects on DNA topology. The religation rate of the relaxed plasmid in the presence of Ru(II) complex **4** is slower than that of complex **5** (Supporting Information). Both complexes **4** and **5** bind to DNA with almost the same affinity and Topo II inhibitory activity, indicating a similar mechanism of molecular action.

■ DISCUSSION

The chalcones can coordinate with *cis*-Ru(DMSO)$_4$Cl$_2$, either by replacing two S-bonded DMSO ligands, or one S-bonded and one O-bonded DMSO ligands, or one DMSO and one chloro ligand. However, owing to the facial arrangement of a
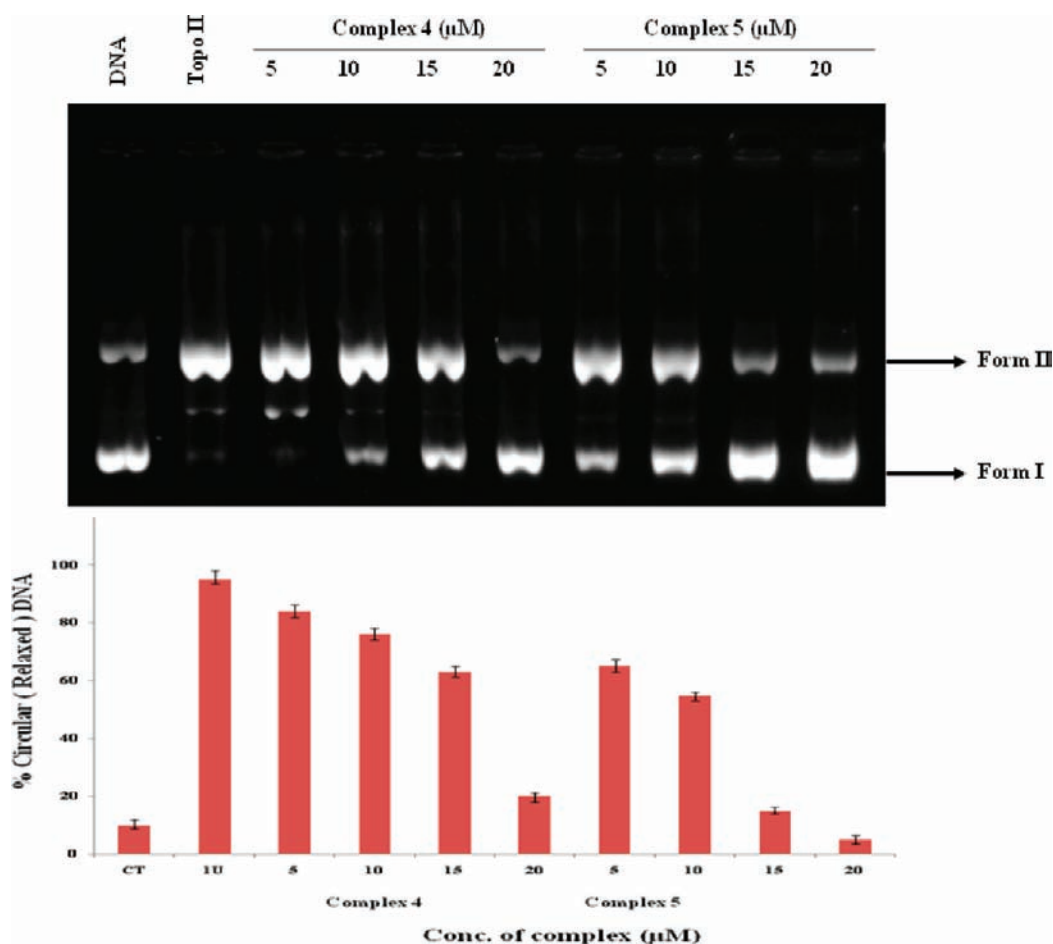
Figure 10. Effects of different concentrations of **4** and **5** on the activity of DNA topoisomerase II.

Table 2. Inhibitory Effects of Complexes 4 and 5 on Activities of Topoisomerase II

	topoisomerase II Inhibitory activity (IC_{50})	ref
camptothecin	>100	60
doxorubicin	1	60
novobiocin	32	60
etoposide	35	60
complex **4**	18	present work
complex **5**	13	present work

chloro and O-bonded DMSO groups, they were substituted by the bidentate deprotonated chalcones chelated as η^2-L (O,O). Two DMSO-S ligands occupy the basal plane, and one chlorine atom and another DMSO-S were bound at axial sites and displayed facial geometry. The unit cell of the complexes contains two discrete molecules, arranged in a head to tail fashion, extending along the axis. In complexes, the chelating chalcones adopt a flattened boat conformation with the H atom on the C^1 in axial position that points toward the S-coordinated DMSO. A computational analysis using PLATON showed that extensive intermolecular C−H···π interactions were displayed from the crystal structure of the complexes (Supporting Information). A weaker molecular force, the CH/π interaction brings the hydrogen bond between soft acids and soft bases, is recognized to play a substantial role in a variety of chemical and biological phenomena.[45] These interactions played a significant role in the building of a supramolecular structure (Supporting Information).[46] Intermolecular C−H(CH_3)···π(phenyl) inter-

actions are responsible for the construction of a linear chain in **1** and **2** at a distance of 2.897 and 2.868 Å, respectively (Supporting Information). Additionally, the crystal structures of **1** and **4** also showed extensive intermolecular C−H···Cl interactions as depicted in the Supporting Information. Complexes **4** and **5** showed intramolecular C−H···S interactions at 2.85 and 2.77 Å distances, respectively (Supporting Information). The packing diagram of complex **5** along the *a*-axis showed formation of a double helical arrangement which looked like a butterfly structure (Supporting Information) supported by cocrystallized water and dichloromethane molecules. The shortest interlayer distance (distance between adjacent Ru···Ru) is observed at 10.5, 8.41, 8.56, 6.84, and 8.35 Å in complexes **1**, **2**, **3**, **4**, and **5**, respectively. These distances are found to be shorter than the distance 12.32 Å, bringing Ru···Ru interactions. The KPI (Kitaigorodskii packing index) values[47] 69.1% with 98 grid points, 69.5% without grid point, 68.8% again without grid points, 68.1% with 60 grid points, and 68.1% with 32 grid points in the complexes **1**, **2**, **3**, **4**, and **5**, respectively, showed compact packing in their crystal lattice.

The most important features of the ^{1}H and ^{13}C NMR spectra of complexes are the following: (i) the coupling constants JH_α−H_β = ~15 Hz in complexes indicating the presence of a trans configuration of ethylinic double bond, while coupling constants of aromatic protons were found in the range J = ~7−8 Hz; (ii) the C-β carbon atom resonance (δ = ~140.41−143.57 ppm) appeared downfield of those of the C-α atoms (δ

~ 121.78 ppm), because of the mesomeric deshielding effect of the carbonyl group.

Spectroelectrochemical Correlation. The UV–vis absorption spectroscopy and cyclic voltammetry can be complementary probes of charge-transfer processes within metal complexes. The MLCT bands in the UV–vis spectrum of metal complexes arise from an electronic excitation which is equivalent to oxidation of the metal ion and reduction of the ligand. The energy of the MLCT transition should equal the absolute difference in potential between corresponding oxidation and reduction processes, as a first approximation. Lever and co-workers[48,49] have demonstrated excellent linear correlations between the MLCT energies. The energy of the MLCT transition could be predicted with the help of observed electrochemical data by considering eqs 3 and 4.[50]

$$\nu_{MLCT} = 8065(\Delta E^\circ) + 3000 \tag{3}$$

$$\Delta E^\circ = E^\circ_{298}(Ru^{III} - Ru^{II}) - E^\circ_{298}(L) \tag{4}$$

ν_{MLCT} is the frequency of the lowest energy MLCT transition (in cm^{-1}). The factor 8065 in eq 3 is used to convert potential difference, ΔE, from volt to cm^{-1}, and the term 3000 cm^{-1} is of empirical origin whereas $E^\circ_{298}(Ru^{III}-Ru^{II})$ and E°_{298} are the formal potentials (in V) of the ruthenium(III)–ruthenium(II) couple as well as the ligand reduction potential, respectively. The calculated and experimentally observed ν_{MLCT} transition frequencies for the complexes are listed in Table 3. The

Table 3. Spectroelectrochemical Correlation Data for Complexes 1−5

complex	E_{298}/V (ΔE_p/mV)		ΔE_c/V	ν_{MLCT}/cm^{-1}	
	Ru^{III}–Ru^{II}	ligand reduction		obsd	calcd
1	0.93	−1.20	2.13	20 243	20 174
2	0.91	−1.28	2.19	20 202	20 660
3	0.79	−1.24	2.03	19 350	19 368
4	0.86	−1.29	2.15	19 841	20 335
5	0.82	−1.32	2.14	19 960	20 254

calculated values lie within 900 cm^{-1} of the experimentally observed energies, which were in very good agreement with the previously observed correlation in other ruthenium complexes.[51]

DNA Binding Studies. Generally, ruthenium complexes form an adduct with DNA which contributes to their cytostatic effect and brings changes in photophysical properties of complexes which in turn have been exploited for monitoring DNA binding properties of the complexes. Significant hypochromicity along with a minor bathochromic shift of MLCT band is observed, suggesting a primarily groove binding nature of the complexes to CT DNA in buffer medium.[52] Small molecules that are known to display π stacking interaction between two DNA base pairs are DNA intercalators which show a much larger bathochromic shift and hypochromic effect of the spectral bands.[53] The more conjugated anthracene ring of the ligand appended in complex 3 provides larger surface area for the interaction with DNA, seems to facilitate partial intercalation with base pair through DNA groove, and results in a higher binding strength than that of complex 1 and 2. On the other hand, complexes 4 and 5, bearing thiophene group in their ligand skeleton, bind strongly with DNA molecule. Thus, the DNA binding potential of these complexes containing simple chalcone ligand framework is found to be comparable

with the Ru(II) complexes bearing a complicated skeleton of porphyrin ligand framework.[54] However, potential binding of complex 5 with DNA could be considered in view of the presence of an electron releasing methyl group attached to thiophene ring in its ligand structures which probably enhances the electron density on the surface of chalcone and concomitantly bring its stronger overlap with symmetrical orbital of DNA bases. As compared to a furan ring containing system, the increase in size of the central atom of the heterocyclic ring increases hydrophobicity and hydrogen binding affinity of DNA together with groove binding affinity, especially at the A−T sequence of DNA.[55] Thus, as expected the role of the thiophene ring is important in bringing the potential candidature of both complexes 4 and 5.

The emission intensity from EB is used as a spectral probe, as it showed enhanced emission intensity when bound to the hydrophobic part of DNA.[56] The binding of complexes to DNA could result in the displacement of the bound EB and could cause a decrease in emission intensity. The K_{sv} values obtained using emission data were found to be similar to that obtained from the absorption titration measurements. Complexes 4 and 5 showed the highest K_{sv} values. It appears that the DNA helix simultaneously accommodates both the complex and EB in the grooves and enhances the hydrophobicity of the thiophene ring in the DNA-bound complex, hence perturbing the DNA helix strongly and displacing the bound EB more efficiently than that of other complexes.

Cleavage Studies. There is substantial and continuous interest in DNA endonucleolytic cleavage reactions that are activated by metal ions. In general, the relaxed form of plasmid DNA is generated due to the cleavage of one of the DNA strands, known as nicking of DNA; the resultant opened circular DNA is known as the nicked circular (form II) form which migrated more slowly in agarose gel. If both strands are cleaved, a linear (form III) form is generated which migrated between I and II forms of DNA.[57] Complexes 4 and 5 exhibited good cleavage activity at 100 μM. However, in the presence of minor groove binding agent DAPI, complexes 4 and 5 showed intense cleavage of DNA even at 20 μM concentration. It suggested a minor groove binding propensity. Additionally, experiments also showed H_2O_2 induced DNA cleavage by complexes 4 and 5 indicating that they followed an oxidative pathway for the cleavage of plasmid DNA.

Under physiological conditions, DNA replication, repair, and transcription processes are significantly controlled by Topo II.[58] The enzyme assists in these functions by altering the topological properties of DNA, and it catalyzes by creating the transient double strand breaks, transporting an intact segment of DNA through the gap, and finally religating the cleaved strands.[59] Two distinct classes of Topo-II inhibitors exist: (1) those that bind to and stabilize the DNA−Topo-II cleavage complex, ultimately promoting the formation of extremely double strand breaks (e.g., etoposide),[60] and (2) those, commonly referred as catalytic inhibitors, that antagonize the ability of the enzyme to perform catalysis (e.g., merbarone).[61] At low complex/DNA ratios, DNA only forms loose aggregates (toroid with gaps), and there are still a number of DNA binding sites in these loose structures accessible for enzymes. However, at high complex/DNA ratios, DNA forms compact aggregates (solid toroid or spherical aggregate), which makes the binding site inaccessible and protects DNA from the digestion of enzymes.[62] The inhibition of topoisomerase largely depends on the nature of the complexes and ligands, and the

presence of uncoordinated sites in the skeleton of coordinated ligands. Both complexes **4** and **5** bind separately to DNA with almost similar affinity and Topo II inhibitory activity, indicating a similar mechanism of molecular action. The precise molecular mechanism of inhibition by these ruthenium complexes remains unknown. It has been well-established that the redox cycling of Fe(thiosemicarbazonato) complexes played a significant role in their ribonucleotide reductase inhibition and cytotoxicity.[63] Indeed, similar results have recently been reported for Cu(thiosemicarbazonato) complexes[64] and for $Ru(II)(C_6H_6)(DMSO)Cl_2$ complex.[17] They inhibit DNA relaxation activity of Topo II by trapping it into a ternary complex with DNA and cross-linking with Topo II. Ruthenium complexes bound covalently to DNA could break the strand in DNA by the generation of free radicals and other oxidation products.[65]

CONCLUSIONS

The present Article embodies the synthesis and characterization of five new complexes of type cis-$[Ru(DMSO)_3L^{1-5}Cl]$ containing different chalcone derivatives (L^{1-5}). The octahedral Ru(II) center prefers the chelating (η^2) binding mode of chalcones. Cyclic voltammetry of the complexes shows that they are redox active in the potential range 0.79−0.93 V. The effect of ring conjugation was quite evident in the extent of binding of corresponding complexes with DNA, monitored using variation in their UV−vis and fluorescence spectra. The DNA-binding ability of the complexes increases with increasing the conjugation in the skeleton of corresponding ligand (**3** > **2** > **1**). However, complexes **4** and **5**, bearing thiophene derivatives in their structural framework, turned out to be the most potential candidates and cleaved supercoiled pBR322 plasmid DNA efficiently following the oxidative pathway. Both complexes prefer minor groove binding as evident from potential cleavage of DNA in the presence of DAPI (DNA minor groove binding agent). Both complexes **4** and **5** inhibited Topo II activity more efficiently than those of many reported inhibitors.

ASSOCIATED CONTENT

Ⓢ Supporting Information

Crystallographic data in CIF format. Additional details, tables, and figures. This material is available free of charge via the Internet at http://pubs.acs.org. CCDC reference numbers 755185, 755186, 834036, 750139, and 78975 contain the supplementary crystallographic data for **1**, **2**, **3**, **4**, and **5**, respectively. These data can be obtained free of charge via http://www.ccdc.cam.ac.uk/conts/retrieving.html, or from the Cambridge Crystallographic Data Centre, 12 Union Road, Cambridge CB2 1EZ, U.K. Fax: (+44) 1223-336-033. E-mail: deposit@ccdc.cam.ac.uk.

AUTHOR INFORMATION

Corresponding Author
*E-mail: lmishrabhu@yahoo.co.in. Phone: +91-542-6702449. Fax: +91-542-2368127.

Notes
The authors declare no competing financial interest.

ACKNOWLEDGMENTS

REFERENCES

(1) Rosenberg, B. *Interdiscip. Sci. Rev.* **1978**, *3*, 134−147.
(2) Brindell, M.; Kuliś, E.; Elmroth, S. K. C.; Urbańska, K.; Stochel, G. *J. Med. Chem.* **2005**, *48*, 7298−7304.
(3) Clarke, M. J. *Coord. Chem. Rev.* **2003**, *236*, 209−233 (and references therein).
(4) *Topics in Biological Inorganic Chemistry*; Sava, G., Alessio, E., Bergamo, A., Mestroni, G., Clarke, M. J., Sadler, P. J., Eds.; Springer: Berlin, 1999; Vol. *1*, pp 143−170.
(5) Ang, W. H.; Dyson, P. J. *Eur. J. Inorg. Chem.* **2006**, 4003−4018.
(6) Manning, G. S. *Q. Rev. Biophys.* **1978**, *11*, 179−246.
(7) Yang, G.; Wu, J. Z.; Wang, L.; Ji, L. N.; Tian, X. *J. Inorg. Biochem.* **1997**, *66*, 141−144.
(8) Ren, J.; Jenkins, T. C.; Chaires, J. B. *Biochemistry* **2000**, *39*, 8439−8447.
(9) Peacock, A. F. A.; Habtemariam, A.; Fernández, R.; Walland, V.; Fabbiani, F. P. A; Parsons, S.; Aird, R. E.; Jodrell, D. I.; Sadler, P. J. *J. Am. Chem. Soc.* **2006**, *128*, 1739−1748.
(10) Yan, Y. K.; Melchart, M.; Habtemariam, A.; Sadler, P. J. *Chem. Commun.* **2005**, 4764−4776.
(11) Scolaro, C.; Bergamo, A.; Brescacin, L.; Delfino, R.; Cocchietto, M.; Laurenczy, G.; Geldbach, T. J.; Sava, G.; Dyson, P. J. *J. Med. Chem.* **2005**, *48*, 4161−4171.
(12) Cusumano, M.; Letizia, M.; Giannetto, A. *Inorg. Chem.* **1999**, *38*, 1754−1758.
(13) Aldrich-Wright, J. R.; Greguric, I. D.; Lau, C. H. Y.; Pellegrini, P.; Collins, J. G. *Recent Res. Dev. Inorg. Chem.* **1998**, *1*, 13−37.
(14) Spence, J. M.; Fournier, R. E. K.; Oshimura, M.; Regnier, V.; Farr, C. J. *Chromosome Res.* **2005**, *13*, 637−648.
(15) Larsen, A. K.; Escargueil, A. E.; Skladanowski, A. *Prog. Cell Cycle Res.* **2003**, *5*, 295−300.
(16) Li, T. K.; Liu, L. F. *Annu. Rev. Pharmacol. Toxicol.* **2001**, *41*, 53−77.
(17) Gopal, Y. N. V.; Konuru, N.; Kondapi, A. K. *Arch. Biochem. Biophys.* **2002**, *401*, 53−62.
(18) Wu, X.; Wilairat, P.; Go, M. L. *Bioorg. Med. Chem. Lett.* **2002**, *12*, 2299−2302.
(19) Daskiewicz, J. B.; Comte, G.; Barron, D.; Petro, A. D.; Thomasson, F. *Tetrahedron Lett.* **1999**, *40*, 7095−7098.
(20) Devincenzo, R.; Scambia, G.; Panici, P. B.; Ranelletti, F. O.; Bonanno, G.; Ercoli, A.; Dellemonache, F.; Ferrari, F.; Piantelli, M.; Mancuso, S. *Anti-Cancer Drug Des.* **1995**, *10*, 481−490.
(21) Wattenberg, L. *J. Cell. Biochem.* **1995**, *22*, 162−168.
(22) Shibata, S. *Stem Cells (Durham, NC, U.S.)* **1994**, *12* (1), 44−52.
(23) Go, M. L.; Wu, X.; Liu, X. L. *Curr. Med. Chem.* **2005**, *12*, 481−499.
(24) Lahtchev, K. L.; Batovska, D. I.; Parushev, St. P; Ubiyvovk, V. M.; Sibirny, A. A. *Eur. J. Med. Chem.* **2008**, *43*, 2220−2228.
(25) Evans, B. E.; Rittle, K. E.; Bock, M. G.; Dipardo, R. M.; Freidinger, R. M.; Whitter, W. L.; Lundell, G. F.; Veber, D. F.; Anderson, P. S.; Chang, R. S. L.; Lotti, V. J.; Cerino, D. J.; Chen, T. B.; Kling, P. J.; Kunkel, K. A.; Springer, J. P.; Hirshfield, J. *J. Med. Chem.* **1988**, *31*, 2235−2246.
(26) Alessio, E.; Mestroni, G.; Nardin, G.; Attia, W. M.; Calligaris, M.; Sava, G.; Zorzet, S. *Inorg. Chem.* **1988**, *27*, 4099−4106.
(27) Raut, K. B.; Wender, S. H. *J. Org. Chem.* **1959**, *25*, 50−52.
(28) Patonay, T.; Jekö, J.; Rimán, É. *Synth. Commun.* **2002**, *32* (15), 2403−2415.
(29) Sheldrick, G. M. *Acta Crystallogr., Sect. A* **2008**, *64*, 112−122.
(30) PLATON: Spek, A. L. *Acta Crystallogr., Sect. D* **2009**, *65*, 148−155.
(31) Marmur, J. *J. Mol. Biol.* **1961**, *3*, 208−218.
(32) Wolfe, A.; Shimer, G. H.; Meehan, T. *Biochemistry* **1987**, *26*, 6392−6396.

(33) Lakowicz, R. *Principles of Fluorescence Spectroscopy*, 2nd ed.; Plenum Press: New York, 1999.

(34) Sukanya, D.; Evans, M. R.; Zeller, M.; Natarajan, K. *Polyhedron* **2007**, *26*, 4314−4320.

(35) Prajapati, R.; Dubey, S. K.; Gaur, R.; Koiri, R. K.; Maurya, B. K.; Trigun, S. K.; Mishra, L. *Polyhedron* **2010**, *29*, 1055−1061.

(36) Rajendiran, V.; Murali, M.; Suresh, E.; Sinha, S.; Somasundaram, K.; Palaniandavar, M. *Dalton Trans.* **2008**, 148−163.

(37) Morris, D. E.; Ohsawa, Y.; Segers, P.; Dearmond, K.; Hanck, K. W. *Inorg. Chem.* **1984**, *23*, 3010−3017.

(38) Mahalingam, V.; Chitrapriya, N.; Fronczek, F. R.; Natarajan, K. *Polyhedron* **2008**, *27*, 1917−1924.

(39) Fischer, B. E.; Sigel, H. *J. Am. Chem. Soc.* **1980**, *102*, 2998−3008.

(40) Greaney, M. A.; Coyle, C. L.; Harmer, M. A.; Jordan, A.; Stiefel, E. I. *Inorg. Chem.* **1989**, *28*, 912−920.

(41) Pyle, A. M.; Rehmann, J. P.; Meshoyrer, R.; Kumar, C. V.; Turro, N. J.; Barton, J. K. *J. Am. Chem. Soc.* **1989**, *111*, 3053−3063.

(42) Zanuy, D.; Alemán, C. *J. Phys. Chem. B* **2008**, *112*, 3222−3230.

(43) Gaur, R.; Khan, R. A.; Tabassum, S.; Shah, P.; Siddiqi, M. I.; Mishra, L. *J. Photochem. Photobiol., A* **2011**, *220*, 145−152.

(44) Chen, G.-J.; Qiao, X.; Tian, J. −L.; Xu, J. −Y.; Gu, W.; Liu, X.; Yan, S.-P. *Dalton Trans.* **2010**, *39*, 10637−10643.

(45) Nishio, M. *Kagaku no Ryoiki* **1979**, *33*, 422−432.

(46) Nunes, C. D.; Pillinger, M.; Hazell, A.; Jepsen, J.; Santos, T. M.; Madureira, J.; Lopes, A. D.; Goncalves, I. S. *Polyhedron* **2003**, *22*, 2799−2807.

(47) Kitaigorodskii, A. I. *Molecular Crystals and Molecules*; Academic Press: New York, 1973.

(48) Lever, A. B. P. *Inorg. Chem.* **1990**, *29*, 1271−1285.

(49) Lever, A. B. P.; Dodsworth, E. S. *Inorganic Electronic Structure and Spectroscopy*; Wiley: New York, 1999; pp 227−290.

(50) Goswami, S.; Mukherjee, R. N.; Chakravorty, A. *Inorg. Chem.* **1983**, *22*, 2825−2832.

(51) Dodsworth, E. S.; Lever, A. B. P. *Chem. Phys. Lett.* **1986**, *124*, 152−158.

(52) Lippert, B. *Coord. Chem. Rev.* **2000**, *200−202*, 487−516.

(53) Chao, H.; Mei, W. J.; Huang, Q. W.; Ji, L. N. *J. Inorg. Biochem.* **2002**, *92*, 165−170.

(54) Rani-Beeram, S.; Meyer, K.; McCrate, A.; Hong, Y.; Nielsen, M.; Swavey, S. *Inorg. Chem.* **2008**, *47*, 11278−11283.

(55) Liu, Y.; Collar, C. J.; Kumar, A.; Stephens, C. E.; Boykin, D. W.; Wilson, W. D. *J. Phys. Chem. B* **2008**, *112*, 11809−11818.

(56) Waring, M. J. *J. Mol. Biol.* **1965**, *13*, 269−282.

(57) Selvakumar, B.; Rajendiran, V.; Maheswari, P. U.; Evans, H. S.; Palaniandavar, M. *J. Inorg. Biochem.* **2006**, *100*, 316−330.

(58) Wang, J. C. *J. Biol. Chem.* **1991**, *266*, 6659−6662.

(59) Vashisht, Y. N. G.; Jayaraju, D.; Kondapi, A. K. *Biochemistry* **1999**, *38*, 4382−4388.

(60) Suzuki, K.; Shono, F.; Uyeda, M. *Biosci. Biotechnol. Biochem.* **1998**, *62*, 2073−2075.

(61) Larsen, A. K.; Escargueil, A. E.; Skladanowski, A. *Pharmacol. Ther.* **2003**, *99* (2), 167−181.

(62) Liu, Y.; Chen, Y.; Duan, Z.-Y.; Feng, X.-Z.; Hou, S.; Wang, C.; Wang, R. *ACS Nano* **2007**, *1* (4), 313−318.

(63) Yu, Y.; Kalinowski, D. S.; Kovacevic, Z.; Siafakas, A. R.; Jansson, P. J.; Stefani, C.; Lovejoy, D. B.; Sharpe, P. C.; Bernhardt, P. V.; Richardson, D. R. *J. Med. Chem.* **2009**, *52*, 5271−5294.

(64) Jansson, P. J.; Sharpe, P. C.; Bernhardt, P. V.; Richardson, D. R. *J. Med. Chem.* **2010**, *53*, 5759−5769.

(65) Clarke, M. J.; Zhu, F.; Frasca, D. R. *Chem. Rev.* **1999**, *99*, 2511−2533.